Predictions of Static Displacements in 1-3 Piezocomposites

L. LI AND N. R. SOTTOS*

Department of Theoretical and Applied Mechanics, University of Illinois at Urbana-Champaign, Urbana, IL 61801

ABSTRACT: Piezocomposites have demonstrated higher sensitivity and lower mechanical losses than single phase piezoelectric materials. As with any composite material, the properties and behavior of piezocomposites are highly dependent on the properties of the constituent materials and the interface between them. In this paper, the micromechanical behavior of 1-3 piezocomposites is investigated. An analytical model is developed for predicting the static displacement behavior of a single piezoelectric rod embedded in a matrix. In the model, the ceramic rod is treated as transversely isotropic since it has different piezoelectric coefficients in the longitudinal and transverse directions.

It is proposed that presence of a thin interlayer or polymer coating around the ceramic rods can influence the longitudinal displacement of the rods and change the overall sensitivity. A composite cylinder model is adopted to incorporate the presence of an interlayer with varying properties. Theoretical predictions indicate that the introduction of a compliant interlayer greatly increases the out-of-plane displacement of the rod and the sensitivity of the composite.

INTRODUCTION

PIEZOELECTRIC ceramics are one class of materials being investigated for use as sensor or actuator elements in smart structures and much attention has been focused on the development of electrically active ceramic-polymer composites. Piezocomposites have demonstrated higher sensitivity and lower mechanical losses than single phase piezoelectric materials. These composites were originally developed for underwater hydrophone applications in the low-frequency range, but have also been extended to other applications such as ultrasonic transducers for acoustic imaging and medical applications. As with any composite material, the properties and behavior of piezocomposites are highly dependent on the properties of the constituent materials and the interface formed between them. The relative compliances of the ceramic and the matrix are particularly important for optimizing the sensitivity. In order to design piezocomposites with optimal sensitivity, the interaction between the polymer matrix and the ceramic must be thoroughly investigated. A variety of piezocomposites can be made by combining a piezoelectric ceramic with a passive polymer. These composites are classified according to their connectivity (Newnham, 1986). Type 1-3 piezocomposites, shown schematically in Figure 1, consist of an array of aligned, piezoelectric ceramic rods embedded in a passive polymer matrix. In the current investigation, the micromechanical behavior of 1-3 piezocomposites is investigated.

Theoretical work concerning the electro-mechanical coupling phenomena in piezocomposites is rather scarce especially in comparison with the numerous micromechanics models which exist on the uncoupled mechanical behavior of traditional or structural composites. Most of the existing works involve the derivation of relations for the effective elastic constants and effective piezoelectric constants of a piezocomposite. Classical models such as the Voigt model which assumes constant strain in the material, and the Reuss model which assumes constant stress, have been utilized (Lees and Davidson, 1977). More refined models include the parallel-serial model (Haun and Newnham, 1986), the cube model (Banno, 1983), and the simple mode by Chan and Unsworth (1989). These simple models are all based on assumptions that either a strain component or the corresponding stress component is constant in the two phases. In addition, Jensen (1991) has used a concentric cylinder model to characterize 1-3 piezocomposites. This model, which estimates the six technically most important constants of the nine constants in the *e*-set, consists of a piezoelectric rod and a concentric elastic tube subjected to axisymmetric load. Because the displacement assumption introduced in this study is the same as the generalized plane strain solution, the concentric tube model also leads to homogeneous strain along the axial direction of the cylinder. Recently, Cao, Zhang and Cross (1992) presented a one-dimensional theoretical study on the static performance of 1-3 piezocomposites. Inhomogeneous displacement profiles were derived for a single-rod composite and a single-tube 1-3 ceramic-polymer composite under uniaxial or hydrostatic stress. Some insight into the fundamental principles of the 1-3 piezocomposite structure, such as the influence of the aspect ratio, was gained through their study.

Micromechanical modeling of piezocomposites is complicated by the fact that the piezoelectric materials exhibit electro-elastic coupling behavior as well as anisotropic behavior. Even for the traditional composites, a three-dimensional micromechanical analysis has not been investi-

*Author to whom correspondence should be addressed.

1045-389X/95/02 0169-12 $10.00/0

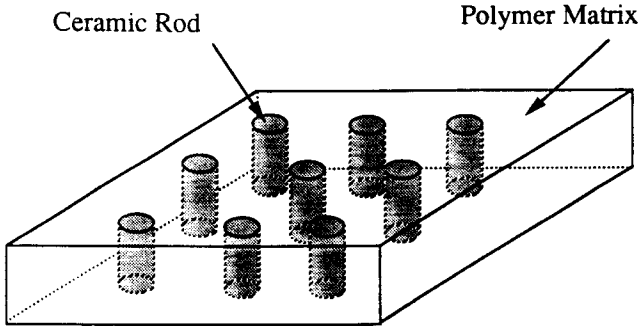

Figure 1. Schematic of a 1-3 piezocomposite.

gated because of the mathematical complexity involved. Whitney and Drzal (1987) developed an approximate closed form solution to predict the axisymmetric stress distribution around a single broken fiber in an unbounded matrix. Their results are derived from an assumed stress function and satisfy the equilibrium and boundary conditions of elasticity exactly, but only satisfy compatibility approximately. Zhong and Folias (1992) examined the 3D stress field of a single cylindrical fiber with finite length embedded in an infinite plate subject to a uniform tensile stress applied to the two ends of the fiber. A three-dimensional solution was achieved by using the method developed by Folias. An edge effect at the fiber ends is observed where the shear stress T_{rz} only satisfies the weak form boundary condition. By using a variational mechanics approach, Nairn (1992) conducted a three-dimensional, axisymmetric stress analysis of the single-fiber fragment of finite length. Like Whitney and Drzal (1987), Nairn's solution only satisfies the compatibility approximately. The investigation notes that the thickness of the boundary layer at the fiber ends is about 0.3 fiber diameter for a fiber fragment of aspect ratio 10.

This paper constitutes a micromechanical analysis of 1-3 piezocomposites. An analytical model is developed for predicting the static displacement behavior of a single piezoelectric rod embedded in a matrix. Development of an analytical model for predicting the displacement behavior of piezoelectric composites is essential in order to optimize constituent properties for maximum sensitivity. In the model, the ceramic rod is treated as transversely isotropic since it has different piezoelectric coefficients in the longitudinal and transverse directions. It is proposed that presence of a thin interlayer or polymer coating around the ceramic rods can influence the longitudinal displacement of the rods and change the overall sensitivity. A composite cylinder model is adopted to incorporate the presence of an interlayer with varying properties. A comparison of the current solution with the simple plane strain models is made. Additionally, a parametric study is performed to systematically examine the influence of interlayer properties and thickness, the influence of matrix properties and the influence of the geometric parameters on the static displacement state of an embedded piezoelectric ceramic rod.

ANALYSIS

Problem Formulation

A schematic of the three-phase composite cylinder used for the analysis is shown in Figure 2. The region $r < r_1$ (ceramic rod), the region $r_1 < r < r_2$ (interlayer) and the region $r_2 < r < r_3$ (embedding polymer matrix) are denoted by superscripts (1), (2) and (3), respectively. The piezoelectric rod is poled in the axial direction (z-direction). The rod is treated as transversely isotropic while the interlayer and the matrix are considered as isotropic and nonpiezoelectric. Any axisymmetric mechanical load or electric field can be applied to the composite model. In the current study, the response of the composite model to a static electrical voltage applied to the ends of the piezoelectric rod is investigated. All the outer surface are assumed to be free of traction.

In cylindrical coordinates, the axially symmetric state of deformation is characterized

$$\begin{cases} u_r^{(i)} = u^{(i)}(r,z) \\ u_\theta^{(i)} = 0 \\ u_z^{(i)} = w^{(i)}(r,z) \end{cases} \qquad (i = 1,2,3) \tag{1}$$

For a transversely isotropic piezoelectric rod the constitutive relations are

$$\begin{cases} T_{rr}^{(1)} = c_{11}^{(1)} S_{rr}^{(1)} + c_{12}^{(1)} S_{\theta\theta}^{(1)} + c_{13}^{(1)} S_{zz}^{(1)} - e_{31}^{(1)} E_z^{(1)} \\ T_{\theta\theta}^{(1)} = c_{12}^{(1)} S_{rr}^{(1)} + c_{11}^{(1)} S_{\theta\theta}^{(1)} + c_{13}^{(1)} S_{zz}^{(1)} - e_{31}^{(1)} E_z^{(1)} \\ T_{zz}^{(1)} = c_{13}^{(1)} S_{rr}^{(1)} + c_{13}^{(1)} S_{\theta\theta}^{(1)} + c_{33}^{(1)} S_{zz}^{(1)} - e_{33}^{(1)} E_z^{(1)} \\ T_{rz}^{(1)} = c_{44}^{(1)} S_{rz}^{(1)} - e_{15}^{(1)} E_r^{(1)} \\ T_{r\theta}^{(1)} = T_{\theta z}^{(1)} = 0 \\ D_r^{(1)} = e_{15}^{(1)} S_{rz}^{(1)} + \epsilon_{11}^{(1)} E_r^{(1)} \\ D_\theta^{(1)} = 0 \\ D_z^{(1)} = e_{31}^{(1)} S_{rr}^{(1)} + e_{31}^{(1)} S_{\theta\theta}^{(1)} + e_{33}^{(1)} S_{zz}^{(1)} + \epsilon_{33}^{(1)} E_z^{(1)} \end{cases} \tag{2}$$

where elastic, dielectric and piezoelectric constants are represented by $c_{\alpha\beta}^{(1)}$, $\epsilon_{\alpha\beta}^{(1)}$ and $e_{\alpha\beta}^{(1)}$ respectively. The interlayer and matrix are isotropic and nonpiezoelectric such that

$$\begin{cases} c_{11}^{(i)} = c_{33}^{(i)} \\ c_{12}^{(i)} = c_{13}^{(i)} \\ c_{44}^{(i)} = \dfrac{1}{2}(c_{11}^{(i)} - c_{12}^{(i)}) \\ e_{31}^{(i)} = e_{33}^{(i)} = e_{15}^{(i)} = 0 \end{cases} \qquad (i = 2,3) \tag{3}$$

The constitutive relations for the interlayer and matrix have the form of

$$\begin{cases} T_{rr}^{(i)} = c_{11}^{(i)} S_{rr}^{(i)} + c_{12}^{(i)} S_{\theta\theta}^{(i)} + c_{12}^{(i)} S_{zz}^{(i)} \\ T_{\theta\theta}^{(i)} = c_{12}^{(i)} S_{rr}^{(i)} + c_{11}^{(i)} S_{\theta\theta}^{(i)} + c_{12}^{(i)} S_{zz}^{(i)} \\ T_{zz}^{(i)} = c_{12}^{(i)} S_{rr}^{(i)} + c_{12}^{(i)} S_{\theta\theta}^{(i)} + c_{11}^{(i)} S_{zz}^{(i)} \quad (i = 2,3) \\ T_{rz}^{(i)} = \frac{1}{2}(c_{11}^{(i)} - c_{12}^{(i)}) S_{rz}^{(i)} \end{cases} \tag{4}$$

Substitution of the constitutive relations and the well known strain-displacement relations into the equilibrium equations and the Gaussian equation gives the following governing equations in terms of displacements and electric field (i = 1,2,3)

$$\begin{cases} c_{11}^{(i)} \left(\frac{\partial^2 u^{(i)}}{\partial r^2} + \frac{1}{r} \frac{\partial u^{(i)}}{\partial r} - \frac{u^{(i)}}{r^2} \right) + (c_{13}^{(i)} + c_{44}^{(i)}) \frac{\partial^2 w^{(i)}}{\partial r \partial z} \\ \qquad + c_{44}^{(i)} \frac{\partial^2 u^{(i)}}{\partial z^2} - e_{31}^{(i)} \frac{\partial E_z^{(i)}}{\partial r} - e_{15}^{(i)} \frac{\partial E_r^{(i)}}{\partial z} = 0 \\ c_{44}^{(i)} \left(\frac{\partial^2 w^{(i)}}{\partial r^2} + \frac{1}{r} \frac{\partial w^{(i)}}{\partial r} \right) + (c_{13}^{(i)} + c_{44}^{(i)}) \\ \qquad \times \left(\frac{\partial^2 u^{(i)}}{\partial r \partial z} + \frac{1}{r} \frac{\partial u^{(i)}}{\partial z} \right) + c_{33}^{(i)} \frac{\partial^2 w^{(i)}}{\partial z^2} \\ \qquad - e_{33}^{(i)} \frac{\partial E_z^{(i)}}{\partial z} - e_{15}^{(i)} \left(\frac{\partial E_r^{(i)}}{\partial r} + \frac{E_r^{(i)}}{r} \right) = 0 \\ e_{15}^{(i)} \left(\frac{\partial^2 w^{(i)}}{\partial r^2} + \frac{1}{r} \frac{\partial w^{(i)}}{\partial r} \right) + (e_{31}^{(i)} + e_{15}^{(i)}) \\ \qquad \times \left(\frac{\partial^2 u^{(i)}}{\partial r \partial z} + \frac{1}{r} \frac{\partial u^{(i)}}{\partial z} \right) + e_{33}^{(i)} \frac{\partial^2 w^{(i)}}{\partial z^2} \\ \qquad + \epsilon_{33}^{(i)} \frac{\partial E_z^{(i)}}{\partial z} + \epsilon_{11}^{(i)} \left(\frac{\partial E_r^{(i)}}{\partial r} + \frac{E_r^{(i)}}{r} \right) = 0 \end{cases} \tag{5}$$

Method of Solution

For the ceramic rod (region 1), the governing equations for mechanical deformation and electric field are coupled. In the current work, it is assumed that the electric field in the ceramic rod can be solved from the electrostatics of a rigid rod. Additionally, the electric field is assumed to be constant in the piezoceramic rod, i.e., $E_z^{(1)} = V/2l$, $E_r^{(1)} = E_\theta^{(1)} = 0$. Due to these assumptions, the three governing equations for the piezoceramic rod are reduced to the following two simplified equations

$$\begin{cases} c_{11}^{(1)} \left(\frac{\partial^2 u^{(1)}}{\partial r^2} + \frac{1}{r} \frac{\partial u^{(1)}}{\partial r} - \frac{u^{(1)}}{r^2} \right) + (c_{13}^{(1)} + c_{44}^{(1)}) \frac{\partial^2 w^{(1)}}{\partial r \partial z} \\ \qquad + c_{44}^{(1)} \frac{\partial^2 u^{(1)}}{\partial z^2} = 0 \\ c_{44}^{(1)} \left(\frac{\partial^2 w^{(1)}}{\partial r^2} + \frac{1}{r} \frac{\partial w^{(1)}}{\partial r} \right) + (c_{13}^{(1)} + c_{44}^{(1)}) \\ \qquad \times \left(\frac{\partial^2 u^{(1)}}{\partial r \partial z} + \frac{1}{r} \frac{\partial u^{(1)}}{\partial z} \right) + c_{33}^{(1)} \frac{\partial^2 w^{(1)}}{\partial z^2} = 0 \end{cases} \tag{6}$$

The complementary solution to Equations (6) for the ceramic rod (i = 1) is achieved by using two displacement potential functions. The displacements are written as (Lekhnitskii, 1981)

$$\begin{cases} u_c^{(1)} = \frac{\partial}{\partial r}(\psi_1 + \psi_2) \\ w_c^{(1)} = \frac{\partial}{\partial z}(s_1 \psi_1 + s_2 \psi_2) \end{cases} \tag{7}$$

The constants s_j (j = 1,2) are determined by

$$s_j = \frac{p_j^2 c_{11}^{(1)} - c_{44}^{(1)}}{c_{13}^{(1)} + c_{44}^{(1)}} \quad (j = 1,2) \tag{8}$$

where p_1^2 and p_2^2 are the roots of the following equation

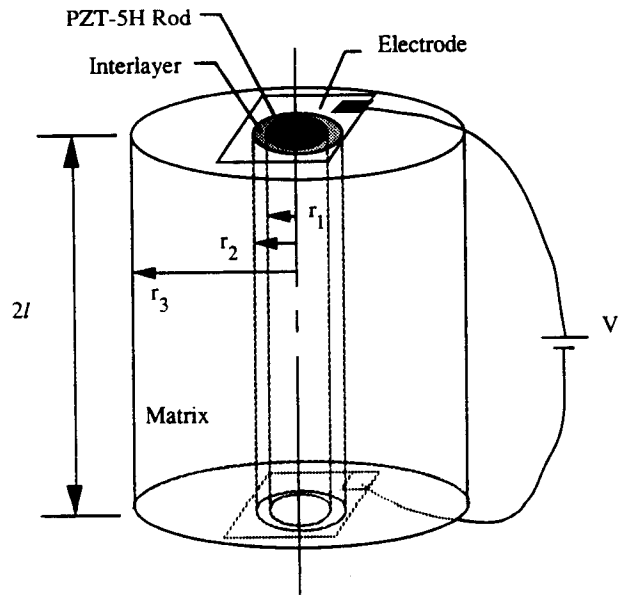

Figure 2. *Schematic of the three phase composite cylinder model.*

$$c_{11}^{(1)}c_{44}^{(1)}p^4 + [c_{13}^{(1)}(c_{13}^{(1)} + 2c_{44}^{(1)}) - c_{11}^{(1)}c_{33}^{(1)}]p^2 + c_{33}^{(1)}c_{44}^{(1)} = 0 \quad (9)$$

In order to satisfy the displacement equations of equilibrium, the potential functions $\psi_1(r,z)$ and $\psi_2(r,z)$ must satisfy the equation

$$\left(\frac{\partial^2}{\partial r^2} + \frac{1}{r}\frac{\partial}{\partial r} + p_j^2\frac{\partial^2}{\partial z^2}\right)\psi_j = 0 \quad (j = 1,2) \quad (10)$$

the solution of which takes the form

$$\begin{cases} \psi_1 = \sum_{n=1}^{\infty} \cos \mu_n z[D_{1n}^{(1)}I_0(p_1\mu_n r) + D_{2n}^{(1)}K_0(p_1\mu_n r)] \\ \psi_2 = \sum_{n=1}^{\infty} \cos \mu_n z[D_{3n}^{(1)}I_0(p_2\mu_n r) + D_{4n}^{(1)}K_0(p_2\mu_n r)] \end{cases} \quad (11)$$

where $D_{1n}^{(1)}$, $D_{2n}^{(1)}$, $D_{3n}^{(1)}$ and $D_{4n}^{(1)}$ are sets of constants and are to be determined from the boundary conditions. The μ_n's are the eigenvalues and determined by the boundary conditions at $z = \pm l$,

$$\mu_n = \frac{n\pi}{2l} \quad (n = 1,3,5,\ldots) \quad (12)$$

The structure of the complementary solution depends on the nature of the value of p_1^2 and p_2^2, and hence depends on the values of the elastic constants. For a PZT-5H rod, p_1^2 and p_2^2 are complex conjugate. Because the displacements and stresses are real and bounded at $r = 0$, the displacement potentials must be complex conjugate functions and are chosen in the form

$$\begin{cases} \psi_1 = \sum_{n=1}^{\infty} \cos \mu_n z\left[D_{1n}^{(1)}I_0(p_1\mu_n r) + \frac{D_{3n}^{(1)}}{i}I_0(p_1\mu_n r)\right] \\ \psi_2 = \sum_{n=1}^{\infty} \cos \mu_n z\left[D_{1n}^{(1)}I_0(\bar{p}_1\mu_n r) - \frac{D_{3n}^{(1)}}{i}I_0(\bar{p}_1\mu_n r)\right] \end{cases} \quad (13)$$

where I_0 is the zero-order modified Bessel function of the first kind and i represents the pure imaginary number, i.e., $i^2 = -1$.

The complementary displacements and stresses for the ceramic rod ($i = 1$) are then obtained as

$$\begin{cases} u_c^{(1)} = \sum_{n=1}^{\infty} \cos (\mu_n z)[D_{1n}^{(1)}h_{1n}^{(1)}(r) + D_{3n}^{(1)}h_{2n}^{(1)}(r)] \\ w_c^{(1)} = \sum_{n=1}^{\infty} \sin (\mu_n z)[D_{1n}^{(1)}h_{3n}^{(1)}(r) + D_{3n}^{(1)}h_{4n}^{(1)}(r)] \\ T_{rr_c}^{(1)} = \sum_{n=1}^{\infty} \cos (\mu_n z)[D_{1n}^{(1)}h_{5n}^{(1)}(r) + D_{3n}^{(1)}h_{6n}^{(1)}(r)] \\ T_{\theta\theta_c}^{(1)} = \sum_{n=1}^{\infty} \cos (\mu_n z)[D_{1n}^{(1)}h_{7n}^{(1)}(r) + D_{3n}^{(1)}h_{8n}^{(1)}(r)] \\ T_{zz_c}^{(1)} = \sum_{n=1}^{\infty} \cos (\mu_n z)[D_{1n}^{(1)}h_{9n}^{(1)}(r) + D_{3n}^{(1)}h_{10n}^{(1)}(r)] \\ T_{rz_c}^{(1)} = \sum_{n=1}^{\infty} \sin (\mu_n z)[D_{1n}^{(1)}h_{11n}^{(1)}(r) + D_{3n}^{(1)}h_{12n}^{(1)}(r)] \end{cases} \quad (14)$$

where functions $h_{1n}^{(1)}(r)$–$h_{12n}^{(1)}(r)$ are given in the Appendix.

For the isotropic and nonpiezoelectric interlayer ($i = 2$) and matrix ($i = 3$) the governing equations, Equations (5), reduce to

$$\begin{cases} \nabla^2 u^{(i)} - \frac{u^{(i)}}{r^2} + \frac{c_{11}^{(i)} + c_{12}^{(i)}}{c_{11}^{(i)} - c_{12}^{(i)}}\frac{\partial}{\partial r} \\ \qquad \times \left(\frac{\partial u^{(i)}}{\partial r} + \frac{u^{(i)}}{r} + \frac{\partial w^{(i)}}{\partial z}\right) = 0 \\ \nabla^2 w^{(i)} + \frac{c_{11}^{(i)} + c_{12}^{(i)}}{c_{11}^{(i)} - c_{12}^{(i)}}\frac{\partial}{\partial r}\left(\frac{\partial u^{(i)}}{\partial r} + \frac{u^{(i)}}{r} + \frac{\partial w^{(i)}}{\partial z}\right) = 0 \end{cases} \quad (15)$$

where

$$\nabla^2 = \frac{\partial^2}{\partial r^2} + \frac{1}{r}\frac{\partial}{\partial r} + \frac{\partial^2}{\partial z^2}$$

The complementary solution to Equations (15) is obtained by using the Love's stress function provided the stress function $F^{(i)}(r,z)$ satisfies the equation,

$$\nabla^2\nabla^2 F^{(i)} = 0 \quad (i = 2,3) \quad (16)$$

It can be shown that the following functions satisfy Equation (16)

$$F^{(i)} = \sum_{n=1}^{\infty} \sin(\mu_n z)\{D_{1n}^{(i)} I_0(\mu_n r) + D_{3n}^{(i)} \mu_n r I_1(\mu_n r) + D_{2n}^{(i)} K_0(\mu_n r) + D_{4n}^{(i)} \mu_n r K_1(\mu_n r)\} \quad (17)$$

where I_0, I_1 and K_0, K_1 are the modified Bessel functions of the first and second kind respectively, while $D_{1n}^{(i)}$, $D_{2n}^{(i)}$, $D_{3n}^{(i)}$ and $D_{4n}^{(i)}$ ($i = 2,3$) are constants to be determined from the boundary conditions. The equations relating Love's function to the complementary displacements and stresses are well known and given in the Appendix. Substitution of $F^{(i)}(r,z)$ into Equations (A14) in the Appendix yields the complementary solution for the interlayer ($i = 2$) and the matrix ($i = 3$),

$$\begin{cases} u_c^{(i)} = \sum_{n=1}^{\infty} \cos(\mu_n z)[D_{1n}^{(i)} h_{1n}^{(i)}(r) + D_{3n}^{(i)} h_{2n}^{(i)}(r) + D_{2n}^{(i)} g_{1n}^{(i)}(r) + D_{4n}^{(i)} g_{2n}^{(i)}(r)] \\ w_c^{(i)} = \sum_{n=1}^{\infty} \sin(\mu_n z)[D_{1n}^{(i)} h_{3n}^{(i)}(r) + D_{3n}^{(i)} h_{4n}^{(i)}(r) + D_{2n}^{(i)} g_{3n}^{(i)}(r) + D_{4n}^{(i)} g_{4n}^{(i)}(r)] \\ T_{rr_c}^{(i)} = \sum_{n=1}^{\infty} \cos(\mu_n z)[D_{1n}^{(i)} h_{5n}^{(i)}(r) + D_{3n}^{(i)} h_{6n}^{(i)}(r) + D_{2n}^{(i)} g_{5n}^{(i)}(r) + D_{4n}^{(i)} g_{6n}^{(i)}(r)] \\ T_{\theta\theta_c}^{(i)} = \sum_{n=1}^{\infty} \cos(\mu_n z)[D_{1n}^{(i)} h_{7n}^{(i)}(r) + D_{3n}^{(i)} h_{8n}^{(i)}(r) + D_{2n}^{(i)} g_{7n}^{(i)}(r) + D_{4n}^{(i)} g_{8n}^{(i)}(r)] \\ T_{zz_c}^{(i)} = \sum_{n=1}^{\infty} \cos(\mu_n z)[D_{1n}^{(i)} h_{9n}^{(i)}(r) + D_{3n}^{(i)} h_{10n}^{(i)}(r) + D_{2n}^{(i)} g_{9n}^{(i)}(r) + D_{4n}^{(i)} g_{10n}^{(i)}(r)] \\ T_{rz_c}^{(i)} = \sum_{n=1}^{\infty} \sin(\mu_n z)[D_{1n}^{(i)} h_{11n}^{(i)}(r) + D_{3n}^{(i)} h_{12n}^{(i)}(r) + D_{2n}^{(i)} g_{11n}^{(i)}(r) + D_{4n}^{(i)} g_{12n}^{(i)}(r)] \end{cases} \quad (18)$$

where $h_{1n}^{(i)}(r)$–$h_{12n}^{(i)}(r)$ are expressions containing r, $I_0(\mu_n r)$ and $I_1(\mu_n r)$, $g_{1n}^{(i)}(r)$–$g_{12n}^{(i)}(r)$ are expressions containing r, $K_0(\mu_n r)$ and $K_1(\mu_n r)$. The functions $h_{1n}^{(i)}(r)$–$h_{12n}^{(i)}(r)$ and $g_{1n}^{(i)}(r)$–$g_{12n}^{(i)}(r)$ ($i = 2,3$) are also given in the Appendix.

The final solution in each region is achieved by superposing the complementary solution and an additional solution corresponding to a generalized plane strain state in order to satisfy all the boundary conditions. The generalized plane strain solution is given by

$$\begin{cases} u_g^{(i)} = A^{(i)} r + \dfrac{B^{(i)}}{r} \\ w_g^{(i)} = \zeta^{(i)} z \\ T_{rr_g}^{(i)} = c_{11}^{(i)}\left(A^{(i)} - \dfrac{B^{(i)}}{r^2}\right) + c_{12}^{(i)}\left(A^{(i)} + \dfrac{B^{(i)}}{r^2}\right) + c_{13}^{(i)}\zeta^{(i)} - e_{31}^{(i)} E_z^{(i)} \\ T_{\theta\theta_g}^{(i)} = c_{12}^{(i)}\left(A^{(i)} - \dfrac{B^{(i)}}{r^2}\right) + c_{11}^{(i)}\left(A^{(i)} + \dfrac{B^{(i)}}{r^2}\right) + c_{13}^{(i)}\zeta^{(i)} - e_{31}^{(i)} E_z^{(i)} \\ T_{zz_g}^{(i)} = 2c_{13}^{(i)} A^{(i)} + c_{33}^{(i)}\zeta^{(i)} - e_{33}^{(i)} E_z^{(i)} \\ T_{rz_g}^{(i)} = T_{\theta z_g}^{(i)} = T_{r\theta_g}^{(i)} = 0 \quad (i = 1,2,3) \end{cases} \quad (19)$$

where $A^{(i)}$, $B^{(i)}$ and $\zeta^{(i)}$ are constants to be determined by boundary conditions.

Boundary Conditions

The total stresses $\underline{\underline{\sigma}} = \underline{\underline{\sigma}}_c + \underline{\underline{\sigma}}_g$ and total displacements $\underline{u} = \underline{u}_c + \underline{u}_g$ are required to satisfy the boundary conditions. The boundary conditions for the single embedded ceramic rod with interlayer shown in Figure 2 are as follows:

1. At $r = 0$ the solution is bounded.
2. At $z = \pm l$ an electric voltage V is applied. The normal traction is zero and the shear stresses constitute a system in equilibrium, so that

$$\begin{cases} T_{zz}^{(1)} = 0 \\ T_{zz}^{(2)} = 0 \\ T_{zz}^{(3)} = 0 \\ \int T_{rz}^{(i)} dr = 0 \end{cases} \quad (20)$$

3. At $r = r_3$ the surface is traction free, i.e.

$$\begin{cases} T_{rr}^{(3)} = 0 \\ T_{rz}^{(3)} = 0 \end{cases} \quad (21)$$

For both the rod-interphase boundary and the interphase-matrix boundary, continuity of displacements and

traction (perfect adhesion) is assumed. Thus the interface boundary conditions are expressed as

4. At $r = r_1$

$$\begin{cases} u^{(1)} = u^{(2)}; & w^{(1)} = w^{(2)} \\ T_{rr}^{(1)} = T_{rr}^{(2)}; & T_{rz}^{(1)} = T_{rz}^{(2)} \end{cases} \tag{22}$$

5. At $r = r_2$

$$\begin{cases} u^{(2)} = u^{(3)}; & w^{(2)} = w^{(3)} \\ T_{rr}^{(2)} = T_{rr}^{(3)}; & T_{rz}^{(2)} = T_{rz}^{(3)} \end{cases} \tag{23}$$

Application of the boundary conditions at $r = 0$ yields

$$B^{(1)} = 0 \tag{24}$$

The remaining boundary conditions generate two systems of linear equations which determine the unknown constants $A^{(1)}$, $A^{(2)}$, $A^{(3)}$, $B^{(2)}$, $B^{(3)}$, $\zeta^{(1)}$, $\zeta^{(2)}$, $\zeta^{(3)}$ and $D_{1n}^{(i)}$, $D_{2n}^{(i)}$, $D_{3n}^{(i)}$, $D_{4n}^{(i)}$.

NUMERICAL RESULTS

Using the solution method outlined above, predictions were made of the static displacements of a single-rod piezoelectric composite assuming the PZT-5H properties listed in Table 1. Geometric parameters are $r_1 = 0.375$ mm, $r_2 = 0.475$ mm, $r_3 = 3$ mm and $l = 5$ mm. The voltage applied to the ends of the composite cylinder is 70 V.

Comparison with Simple Models

The axial displacement at $z = l$ of the piezocomposite cylinder is first calculated for the case of no interlayer. Displacement values are compared with those predicted by simple plane strain models (Haun and Newnham, 1986; Chan and Unsworth, 1989; Jensen, 1991) and are plotted as a function of radial distance in Figure 3. The displacement profile obtained according to the simple models is uniform because all of these models give the same prediction of the effective composite piezoelectric constant, $\bar{d}_{33}$, which is expressed

$$\bar{d}_{33} = \frac{v_f d_{33}^{(1)} s_{33}^{(3)}}{v_f s_{33}^{(3)} + (1 - v_f) s_{33}^{(1)}} \tag{25}$$

where v_f is the volume fraction of piezoelectric ceramic rods and $s_{\alpha\beta}^{(i)}$ are elastic compliance constants for each phase. When a 1-3 piezocomposite in these simple models is subjected to uniform axial electric field (E_z) only, the axial strain is given by $\bar{S}_{zz} = \bar{d}_{33} E_z$ and the axial displacement is $w = \bar{S}_{zz} z$.

The current solution predicts a non-uniform displacement profile. The maximum displacement occurs in the rod and decreases rapidly with radial distance in the matrix. As the length of the rod $2l$, approaches infinity (continuous rods), the solution approaches that of a generalized plane strain model such as the concentric cylinder model by Jensen (1991).

Table 1. Elastic and piezoelectric properties of PZT-5H rod.

Piezoceramic	PZT 5H	Piezoceramic	PZT 5H
$c_{11}^{(1)}$ (GPa)	126	e_{31} (C/m²)	−6.55
$c_{12}^{(1)}$ (GPa)	79.5	e_{33} (C/m²)	23.3
$c_{13}^{(1)}$ (GPa)	84.1	e_{15} (C/m²)	17.0
$c_{33}^{(1)}$ (GPa)	117	d_{31} (10^{-12} m/V)	−274
$c_{44}^{(1)}$ (GPa)	23.0	d_{33} (10^{-12} m/V)	593

Influence of the Interlayer Properties

A parametric study was carried out to systematically assess the influence of the interlayer properties on the static displacement of the current 1-3 piezocomposite model. The interlayer was chosen to have an elastic stiffness either higher or lower than the neat matrix. The properties of the various interlayers used in the calculations are given in Table 2. The properties of the surrounding matrix are kept as $c_{11}^{(3)} = 2.87$ GPa and $c_{12}^{(3)} = 1.211$ GPa. The $Y^{(2)}$ in Table 2 is the Young's modulus of the interlayer and $\nu^{(2)}$ is the Poisson's ratio. Four different cases were considered. In case 1 the interlayer and the matrix are the same. In case 2 the interlayer is softer than the matrix, $Y^{(2)} = (1/5)Y^{(3)}$, while in case 3 the interlayer is stiffer than the matrix, $Y^{(2)} = 5Y^{(3)}$. In case 4, the interlayer is very compliant, $Y^{(2)} = (1/100)Y^{(3)}$. The matrix is assumed to be Spurr epoxy and the properties were calculated using data from the manufacturer and room temperature tension tests.

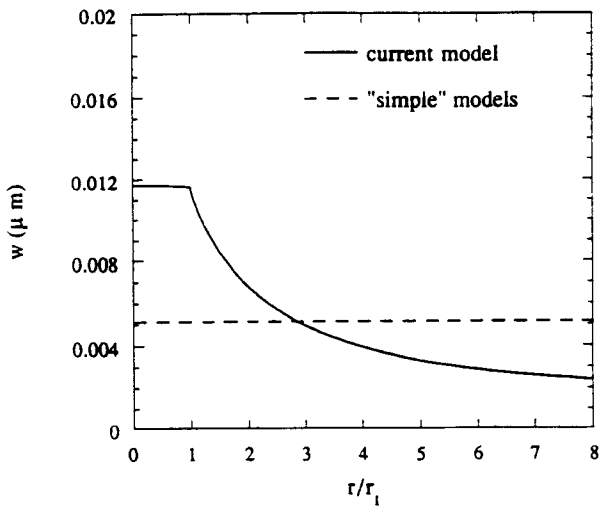

Figure 3. Predictions using the current model and simple plane strain models of axial displacement at z = l.

Table 2. Elastic properties of interlayer used for parametric studies.

Property	Case 1	Case 2	Case 3	Case 4
$c_{11}^{(2)}$ (GPa)	2.827	0.565	14.135	0.0287
$c_{12}^{(2)}$ (GPa)	1.211	0.242	6.055	0.01211
$Y^{(2)}$ (GPa)	2.101	0.420	10.50	0.021
$\nu^{(2)}$	0.3	0.3	0.3	0.3

Table 3. Elastic properties of matrix.

Property	Case 1	Case 5	Case 6
$c_{11}^{(3)}$ (GPa)	2.827	0.565	14.135
$c_{12}^{(3)}$ (GPa)	1.211	0.242	6.055
$Y^{(3)}$ (GPa)	2.101	0.420	10.50
$\nu^{(3)}$	0.3	0.3	0.3

Axial displacement profiles at $z = l$ of the piezocomposite cylinder corresponding to interlayers with various elastic properties are shown in Figure 4. In the calculation, the parameters of r_1, r_2, r_3, l and V remain unchanged. The out-of-plane displacement of the piezocomposite is significantly influenced by introducing an interlayer with a thickness of only 0.1 mm. The axial displacement of the PZT rod increases as the modulus of the interlayer decreases. The maximum displacement of the rod can be increased by 64% by reducing the interlayer modulus to one hundredth of the matrix modulus.

Influence of the Matrix Properties

The influence of the matrix on static displacements was examined by keeping the interlayer properties constant while varying the matrix properties. Three different cases were considered. Properties of the matrix are tabulated in Table 3 and the results are shown in Figure 5. In case 1 the interlayer and the matrix are the same. In case 5 the matrix is softer than the interlayer while in case 6 the matrix is stiffer than the interlayer. An interlayer with constant properties $c_{11}^{(2)} = 2.827$ GPa and $c_{12}^{(2)} = 1.211$ GPa is assumed for the calculations and the parameters of r_1, r_2, r_3, l and V remain unchanged. The out-of-plane displacement of the single-rod piezocomposite is highly dependent on the modulus of matrix. The trend of displacement variation shown in Figure 5 agrees with that predicted by simple models, i.e., a composite with lower matrix modulus has a larger displacement.

Influence of the Interlayer Thickness

The study of interaction between the polymer matrix, the interphase and the piezoelectric ceramic was further developed by investigating the influence of interlayer thickness on the displacement profile. Thickness variations were studied for both a soft interlayer (case 2 in Table 2) and a stiff interlayer (case 3 in Table 2). The thickness of the interlayer is defined as $\lambda = r_2 - r_1$. The maximum axial displacement which is achieved at the center of the rod is plotted versus λ in Figures 6a and 6b. For a soft interlayer, the maximum displacement increases as λ increases. For a stiff interlayer, the displacement decreases as λ increases. The results show that the influence of the interlayer becomes more significant as the thickness of the interlayer increases.

Influence of the Ceramic Rod Volume Fraction

Volume fraction of ceramic rods is an important parameter for designing and evaluating piezocomposites. In the

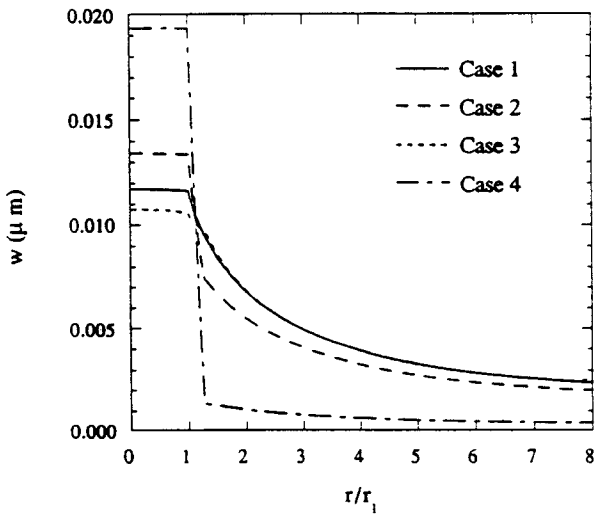

Figure 4. Axial displacement profiles at z = l for interlayers of varying moduli and thickness of λ = 0.1 mm.

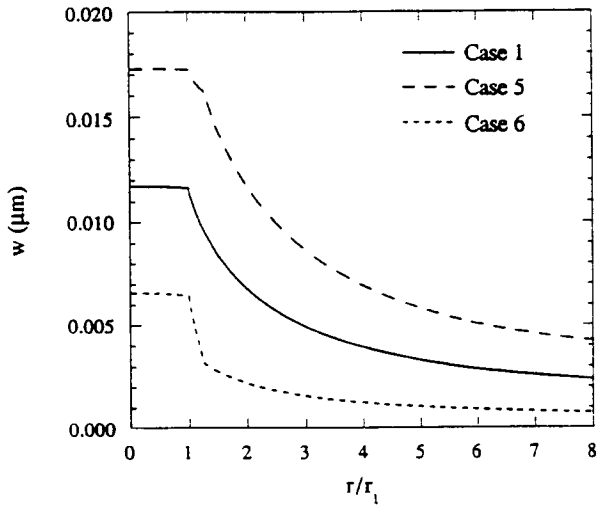

Figure 5. Axial displacement profiles at z = l for matrices of varying moduli (λ = 0.1 mm).

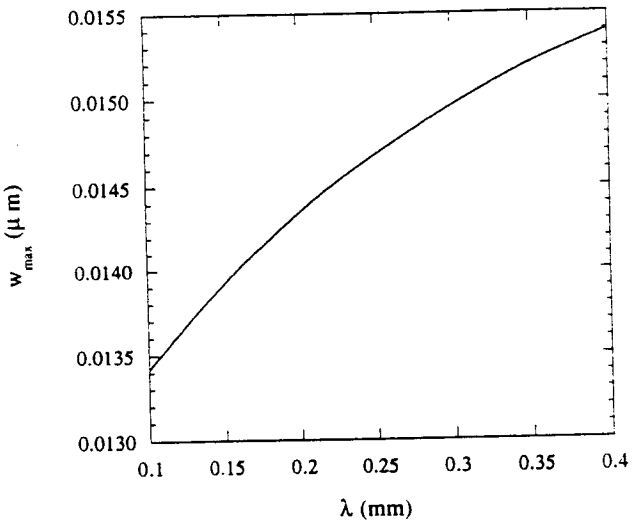

Figure 6a. *Variation of the maximum axial rod displacement with interlayer thickness, λ, for a soft interlayer ($Y^{(2)} = Y^{(3)}/5$).*

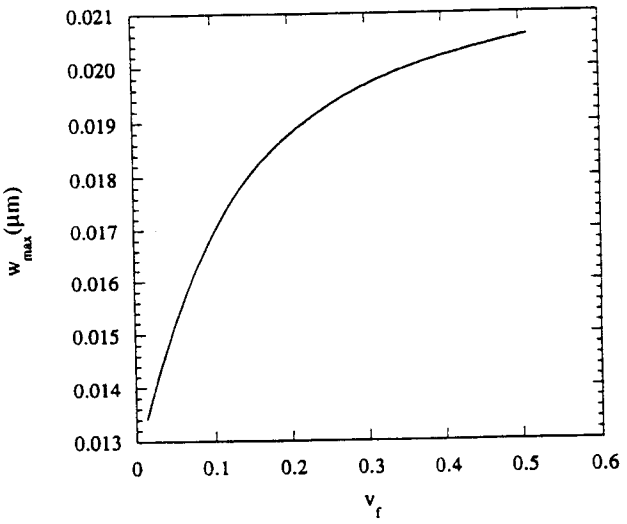

Figure 7. *Variation of the maximum axial rod displacement with volume fraction of PZT rods.*

current single-rod model, the volume fraction of rods is calculated by $v_f = (r_1/r_3)^2$. The effect of increasing rod volume fraction is shown in Figure 7 where maximum axial displacement is plotted as a function of v_f. Interlayer and matrix parameters used in the calculation correspond to case 2 in Table 2. As the volume fraction of rods increases, the maximum displacement also increases.

Calculation of the Effective Piezoelectric Constants

The current solution can also be used to estimate the effective properties of the piezocomposite. The piezoelectric charge constants $\bar{d}_{33}$ and $\bar{d}_{31}$ are calculated by dividing the volume average axial strain and volume average radial strain by the applied electric field, respectively. Figure 8 shows the influence of the PZT rod aspect ratio on the effective piezoelectric constants $\bar{d}_{33}$ and $\bar{d}_{31}$ for the case of no interlayer. The volume fraction of the PZT rods is 25%. As the rods become shorter, the values of $\bar{d}_{33}$ and $\bar{d}_{31}$ decrease from those predicted by simple models for composites with infinitely long rods. The effective hydrostatic constant for the composite, $\bar{d}_h$, can be calculated from $\bar{d}_{33}$ and $-\bar{d}_{31}$ as $\bar{d}_h = \bar{d}_{33} + 2\bar{d}_{31}$. In Figure 9, $\bar{d}_h$ is plotted as a function of v_f for the case of no interlayer. The PZT rod aspect ratio, $r_1/2l$, is 0.1. A maximum value is observed at about 35% for the current model.

The solution is also compared to the simple plane strain model as well as the one-dimensional model by Cao, Zhang and Cross (1992). For a fixed volume fraction of PZT rods, the simple plane strain model gives the highest prediction of

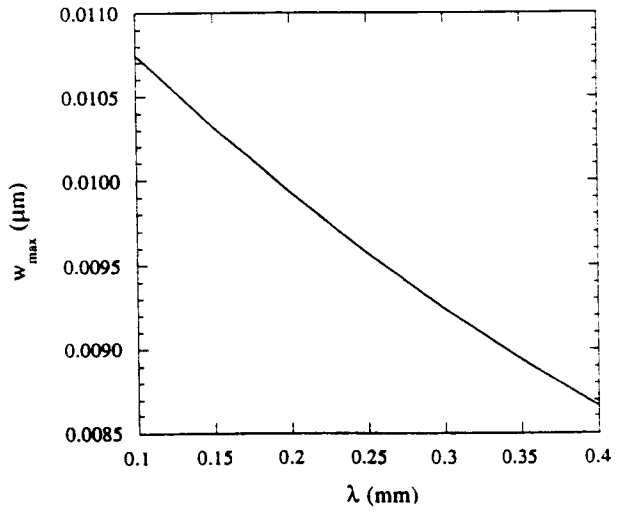

Figure 6b. *Variation of the maximum axial rod displacement with interlayer thickness, λ, for a stiff interlayer ($Y^{(2)} = 5 * Y^{(3)}$).*

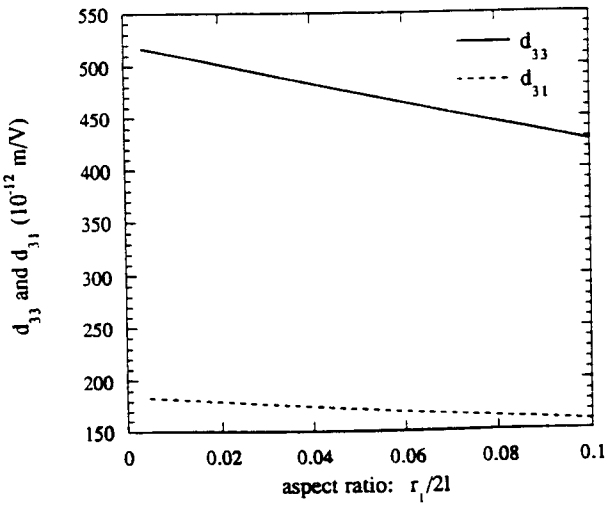

Figure 8. *Variation of effective charge constants with PZT rod aspect ratio, $v_f = 0.25$.*

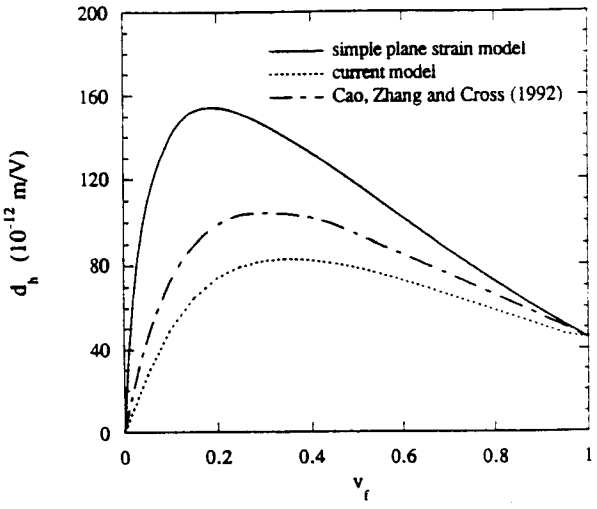

Figure 9. *Predictions of $\bar{d}_h$ using the current model, the simple plane strain model and the one-dimensional model of Cao, Zhang and Cross (1992) for the case of no interlayer and $r_1/2l = 0.1$.*

$\bar{d}_h$. The assumption of isostrain in the axial direction is abandoned in the one-dimensional model, but the assumption of isostress in the lateral direction is still retained. Thus, the prediction of $\bar{d}_h$ made from the one-dimensional model by Cao, Zhang and Cross (1992) is greater than the value from the current model.

The influence of the interlayer modulus on $\bar{d}_{33}$ and $-\bar{d}_{31}$ are plotted in Figure 10 as a function of the ratio of the interlayer modulus and the matrix modulus. The volume fraction of the PZT rods is fixed at 25%. Both $\bar{d}_{33}$ and $-\bar{d}_{31}$ decrease as the interlayer becomes more compliant. In Figure 11, $\bar{d}_h$ is plotted as a function of interlayer modulus. For a volume fraction of 25%, $\bar{d}_h$ increases as the interlayer becomes more compliant.

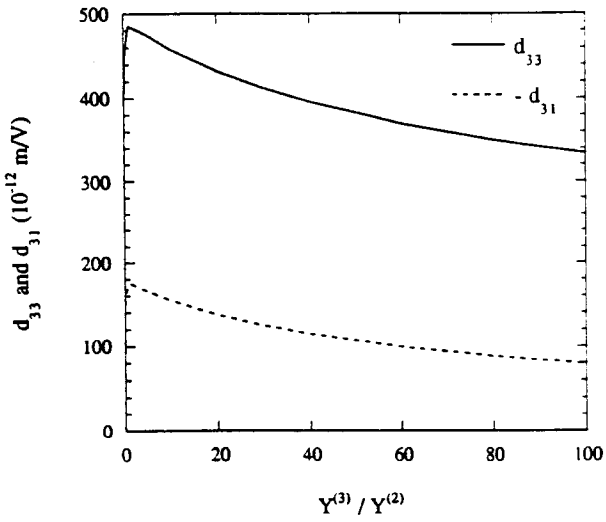

Figure 10. *Variation of effective charge constants with interlayer modulus for an interphase thickness of $\lambda = 0.1$ mm, $v_f = 0.25$.*

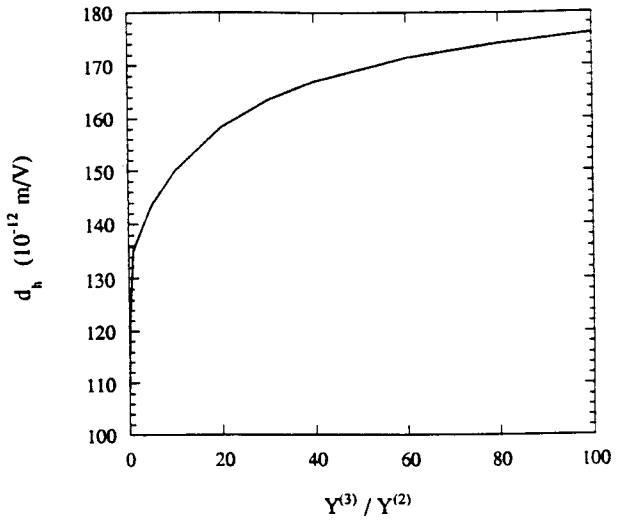

Figure 11. *Variation of the effective hydrostatic charge coefficient, d_h, with interlayer modulus for $\lambda = 0.1$ mm, $v_f = 0.25$.*

CONCLUSIONS

Difficulties exist in manufacturing 1-3 piezocomposites with small $r_1/2l$ ratio, where r_1 is radius of the ceramic rod and $2l$ is length of the composite. In practice, values of $r_1/2l$ are typically larger than 0.02. Thus, 1-3 piezocomposites should be modeled as aligned short fiber composites not as continuous fiber composites. In the current work, a three-dimensional analytical model was developed for studying the static displacement behavior of a finite single-rod piezocomposite. The method employed can also be used to study the stress state, the load transfer behavior and the electric field concentration in 1-3 piezocomposites.

The results obtained using the current model demonstrate that the out-of-plane displacements of the composite are highly dependent on the interaction between the polymer matrix, a thin interlayer and the piezoelectric ceramic. In order to enhance the out-of-plane displacement, a passive matrix with small Young's modulus should be chosen. This result is similar to that obtained from simple models. However, the overall stiffness of the composite is dependent on the matrix modulus, especially for lower volume fractions. By introducing a thin compliant interlayer, the out-of-plane displacement of the rod is greatly increased while the requirement for overall stifffness of the composite can still be satisfied. The interlayer essentially serves to couple or decouple the rods from the matrix, depending on its stiffness. Interlayer properties were also found to significantly influence the effective charge constants for the piezocomposite. Both $\bar{d}_{33}$ and $-\bar{d}_{31}$ decrease with decreasing interlayer stiffness. Because the decrease in $-\bar{d}_{31}$ is larger than the corresponding decrease in $\bar{d}_{33}$, the effective hydrostatic constant for the composite increases for a lower modulus interlayer. Thus, the interlayer can be tailored to optimize the properties and increase the sensitivity of 1-3 piezocomposites.

ACKNOWLEDGEMENT

The support of the Office of Naval Research is greatly appreciated. This work was supported under grant N00014-92-J-1620.

APPENDIX

In region 1 the complementary displacements and stresses (denoted by subscript c) are related to the displacement potential functions $\psi_1(r,z)$ and $\psi_2(r,z)$ by

$$\begin{cases} u_c^{(1)} = \dfrac{\partial}{\partial r}(\psi_1 + \psi_2) \\ w_c^{(1)} = \dfrac{\partial}{\partial z}(s_1\psi_1 + s_2\psi_2) \\ T_{rr_c}^{(1)} = -\dfrac{c_{11}^{(1)} - c_{12}^{(1)}}{r}\dfrac{\partial}{\partial r}(\psi_1 + \psi_2) \\ \qquad - c_{44}^{(1)}\dfrac{\partial^2}{\partial z^2}[(1 + s_1)\psi_1 + (1 + s_2)\psi_2] \\ T_{\theta\theta_c}^{(1)} = \dfrac{c_{11}^{(1)} - c_{12}^{(1)}}{r}\dfrac{\partial}{\partial r}(\psi_1 + \psi_2) \\ \qquad + \dfrac{\partial^2}{\partial z^2}[(c_{13}^{(1)}s_1 - c_{12}^{(1)}p_1^2)\psi_1 + (c_{13}^{(1)}s_2 - c_{12}^{(1)}p_2^2)\psi_2] \\ T_{zz_c}^{(1)} = \dfrac{\partial^2}{\partial z^2}[(c_{33}^{(1)}s_1 - c_{13}^{(1)}p_1^2)\psi_1 + (c_{33}^{(1)}s_2 - c_{13}^{(1)}p_2^2)\psi_2] \\ T_{rz_c}^{(1)} = c_{44}^{(1)}\dfrac{\partial^2}{\partial r\partial z}[(1 + s_1)\psi_1 + (1 + s_2)\psi_2] \end{cases} \tag{A1}$$

The functions $h_{jn}^{(1)}$, where $j = 1,2,\ldots 12$ in Equations (14) can be expressed in terms of modified Bessel functions of the first kind I_0, I_1 and elastic constants of the piezoelectric ceramic as follows,

$$h_{1n}^{(1)}(r) = p_1\mu_n I_1(p_1\mu_n r) + \bar{p}_1\mu_n I_1(\bar{p}_1\mu_n r) \tag{A2}$$

$$h_{2n}^{(1)}(r) = \frac{1}{i}[p_1\mu_n I_1(p_1\mu_n r) - \bar{p}_1\mu_n I_1(\bar{p}_1\mu_n r)] \tag{A3}$$

$$h_{3n}^{(1)}(r) = -\mu_n[s_1 I_0(p_1\mu_n r) + \bar{s}_1 I_0(\bar{p}_1\mu_n r)] \tag{A4}$$

$$h_{4n}^{(1)}(r) = -\frac{\mu_n}{i}[s_1 I_0(p_1\mu_n r) - \bar{s}_1 I_0(\bar{p}_1\mu_n r)] \tag{A5}$$

$$\begin{aligned} h_{5n}^{(1)}(r) = {} & c_{44}^{(1)}\mu_n^2[I_0(p_1\mu_n r) + I_0(\bar{p}_1\mu_n r) \\ & + s_1 I_0(p_1\mu_n r) + \bar{s}_1 I_0(\bar{p}_1\mu_n r)] \\ & - \frac{c_{11}^{(1)} - c_{12}^{(1)}}{r}[p_1\mu_n I_1(p_1\mu_n r) + \bar{p}_1\mu_n I_1(p_1\mu_n r)] \end{aligned} \tag{A6}$$

$$\begin{aligned} h_{6n}^{(1)}(r) = {} & \frac{c_{44}^{(1)}\mu_n^2}{i}[I_0(p_1\mu_n r) - I_0(\bar{p}_1\mu_n r) \\ & + s_1 I_0(p_1\mu_n r) - \bar{s}_1 I_0(\bar{p}_1\mu_n r)] \\ & - \frac{c_{11}^{(1)} - c_{12}^{(1)}}{ir}[p_1\mu_n I_1(p_1\mu_n r) + \bar{p}_1\mu_n I_1(p_1\mu_n r)] \end{aligned} \tag{A7}$$

$$\begin{aligned} h_{7n}^{(1)}(r) = {} & \frac{c_{11}^{(1)} - c_{12}^{(1)}}{r}[p_1\mu_n I_1(p_1\mu_n r) + \bar{p}_1\mu_n I_1(p_1\mu_n r)] \\ & - \mu_n^2(c_{13}^{(1)}s_1 - c_{12}^{(1)}p_1^2)I_0(p_1\mu_n r) \\ & - \mu_n^2(c_{13}^{(1)}\bar{s}_1 - c_{12}^{(1)}\bar{p}_1^2)\bar{I}_0(p_1\mu_n r) \end{aligned} \tag{A8}$$

$$\begin{aligned} h_{8n}^{(1)}(r) = {} & \frac{c_{11}^{(1)} - c_{12}^{(1)}}{ir}[p_1\mu_n I_1(p_1\mu_n r) + \bar{p}_1\mu_n I_1(p_1\mu_n r)] \\ & - \frac{\mu_n^2}{i}(c_{13}^{(1)}s_1 - c_{12}^{(1)}p_1^2)I_0(p_1\mu_n r) \\ & + \frac{\mu_n^2}{i}(c_{13}^{(1)}\bar{s}_1 - c_{12}^{(1)}\bar{p}_1^2)\bar{I}_0(p_1\mu_n r) \end{aligned} \tag{A9}$$

$$\begin{aligned} h_{10n}^{(1)}(r) = {} & -\mu_n^2[(c_{33}^{(1)}s_1 - c_{13}^{(1)}p_1^2)I_0(p_1\mu_n r) \\ & + (c_{33}^{(1)}\bar{s}_1 - c_{13}^{(1)}\bar{p}_1^2)\bar{I}_0(p_1\mu_n r)] \end{aligned} \tag{A10}$$

$$\begin{aligned} h_{10n}^{(1)}(r) = {} & -\frac{\mu_n^2}{i}[(c_{33}^{(1)}s_1 - c_{13}^{(1)}p_1^2)I_0(p_1\mu_n r) \\ & - (c_{33}^{(1)}\bar{s}_1 - c_{13}^{(1)}\bar{p}_1^2)\bar{I}_0(p_1\mu_n r)] \end{aligned} \tag{A11}$$

$$\begin{aligned} h_{11n}^{(1)}(r) = {} & -c_{44}^{(1)}\mu_n[p_1\mu_n I_1(p_1\mu_n r) + \bar{p}_1\mu_n\bar{I}_1(p_1\mu_n r) \\ & + s_1 p_1\mu_n I_1(p_1\mu_n r) + \bar{s}_1\bar{p}_1\mu_n\bar{I}_1(p_1\mu_n r)] \end{aligned} \tag{A12}$$

$$\begin{aligned} h_{12n}^{(1)}(r) = {} & -\frac{c_{44}^{(1)}}{i}\mu_n[p_1\mu_n I_1(p_1\mu_n r) - \bar{p}_1\mu_n\bar{I}_1(p_1\mu_n r) \\ & + s_1 p_1\mu_n I_1(p_1\mu_n r) - \bar{s}_1\bar{p}_1\mu_n\bar{I}_1(p_1\mu_n r)] \end{aligned} \tag{A13}$$

Note in Equations (A2) to (A13) i only represents the pure imaginary number, i.e., $i^2 = -1$.

In region 2 and region 3 the complementary solution for the displacements and stresses are of the form

$$u_c^{(i)} = -\frac{1}{c_{11}^{(i)} - c_{12}^{(i)}} \frac{\partial^2 F^{(i)}}{\partial r \partial z}$$

$$w_c^{(i)} = \frac{1}{c_{11}^{(i)} - c_{12}^{(i)}} \left[\frac{2c_{11}^{(i)}}{c_{11}^{(i)} + c_{12}^{(i)}} \nabla^2 F^{(i)} - \frac{\partial^2 F^{(i)}}{\partial z^2} \right]$$

$$T_{rr_c}^{(i)} = \frac{\partial}{\partial z} \left[\frac{c_{12}^{(i)}}{c_{11}^{(i)} + c_{12}^{(i)}} \nabla^2 F^{(i)} - \frac{\partial^2 F^{(i)}}{\partial r^2} \right]$$

$$T_{\theta\theta_c}^{(i)} = \frac{\partial}{\partial z} \left[\frac{c_{12}^{(i)}}{c_{11}^{(i)} + c_{12}^{(i)}} \nabla^2 F^{(i)} - \frac{1}{r} \frac{\partial F^{(i)}}{\partial r} \right] \quad \text{(A14)}$$

$$T_{zz_c}^{(i)} = \frac{\partial}{\partial z} \left[\frac{2c_{11}^{(i)} + c_{12}^{(i)}}{c_{11}^{(i)} + c_{12}^{(i)}} \nabla^2 F^{(i)} - \frac{\partial^2 F^{(i)}}{\partial z^2} \right]$$

$$T_{rz_c}^{(i)} = \frac{\partial}{\partial z} \left[\frac{c_{11}^{(i)}}{c_{11}^{(i)} + c_{12}^{(i)}} \nabla^2 F^{(i)} - \frac{\partial^2 F^{(i)}}{\partial z^2} \right]$$

where $F^{(i)}$ is Love's displacement potential and the superscript $i = 2,3$ for the interlayer and matrix region respectively. The functions $h_{jn}^{(i)}$ and $g_{jn}^{(i)}$, where $i = 2,3$ and $j = 1,2,\ldots 12$ in Equations (18) can be expressed in terms of modified Bessel functions of the first and second I_0, I_1, K_0, K_1 and the elastic constants as follows:

$$h_{1n}^{(i)} = -\left(\frac{1}{c_{11}^{(i)} - c_{12}^{(i)}} \right) \mu_n^2 I_1(\mu_n r) \quad \text{(A15)}$$

$$h_{2n}^{(i)} = -\left(\frac{1}{c_{11}^{(i)} - c_{12}^{(i)}} \right) \mu_n^3 r I_0(\mu_n r) \quad \text{(A16)}$$

$$h_{3n}^{(i)} = \left(\frac{1}{c_{11}^{(i)} - c_{12}^{(i)}} \right) \mu_n^2 I_0(\mu_n r) \quad \text{(A17)}$$

$$h_{4n}^{(i)} = \left(\frac{\mu_n^2}{c_{11}^{(i)} - c_{12}^{(i)}} \right) \left[\frac{4c_{11}^{(i)}}{c_{11}^{(i)} + c_{12}^{(i)}} I_0(\mu_n r) + \mu_n r I_1(\mu_n r) \right] \quad \text{(A18)}$$

$$h_{5n}^{(i)} = \mu_n^2 \left[-\mu_n I_0(\mu_n r) + \frac{1}{r} I_1(\mu_n r) \right] \quad \text{(A19)}$$

$$h_{6n}^{(i)} = \mu_n^3 \left[\left(\frac{c_{12}^{(i)} - c_{11}^{(i)}}{c_{11}^{(i)} + c_{12}^{(i)}} \right) I_0(\mu_n r) - \mu_n r I_1(\mu_n r) \right] \quad \text{(A20)}$$

$$h_{7n}^{(i)} = -\frac{\mu_n^2}{r} I_1(\mu_n r) \quad \text{(A21)}$$

$$h_{8n}^{(i)} = \mu_n^3 \left(\frac{c_{12}^{(i)} - c_{11}^{(i)}}{c_{11}^{(i)} + c_{12}^{(i)}} \right) I_0(\mu_n r) \quad \text{(A22)}$$

$$h_{9n}^{(i)} = \mu_n^3 I_0(\mu_n r) \quad \text{(A23)}$$

$$h_{10n}^{(i)} = \mu_n^3 \left[\left(\frac{4c_{11}^{(i)} + 2c_{12}^{(i)}}{c_{11}^{(i)} + c_{12}^{(i)}} \right) I_0(\mu_n r) + \mu_n r I_1(\mu_n r) \right] \quad \text{(A24)}$$

$$h_{11n}^{(i)} = \mu_n^3 I_1(\mu_n r) \quad \text{(A25)}$$

$$h_{12n}^{(i)} = \mu_n^3 \left[\left(\frac{2c_{11}^{(i)}}{c_{11}^{(i)} + c_{12}^{(i)}} \right) I_1(\mu_n r) + \mu_n r I_0(\mu_n r) \right] \quad \text{(A26)}$$

$$g_{1n}^{(i)} = \left(\frac{1}{c_{11}^{(i)} - c_{12}^{(i)}} \right) \mu_n^2 K_1(\mu_n r) \quad \text{(A27)}$$

$$g_{2n}^{(i)} = \left(\frac{1}{c_{11}^{(i)} - c_{12}^{(i)}} \right) \mu_n^3 r K_0(\mu_n r) \quad \text{(A28)}$$

$$g_{3n}^{(i)} = \left(\frac{1}{c_{11}^{(i)} - c_{12}^{(i)}} \right) \mu_n^2 K_0(\mu_n r) \quad \text{(A29)}$$

$$g_{4n}^{(i)} = \left(\frac{\mu_n^2}{c_{11}^{(i)} - c_{12}^{(i)}} \right) \left[\frac{-4c_{11}^{(i)}}{c_{11}^{(i)} + c_{12}^{(i)}} K_0(\mu_n r) + \mu_n r K_1(\mu_n r) \right] \quad \text{(A30)}$$

$$g_{5n}^{(i)} = \mu_n^2 \left[-\mu_n K_0(\mu_n r) - \frac{1}{r} K_1(\mu_n r) \right] \quad \text{(A31)}$$

$$g_{6n}^{(i)} = \mu_n^3 \left[\left(\frac{c_{11}^{(i)} - c_{12}^{(i)}}{c_{11}^{(i)} + c_{12}^{(i)}} \right) K_0(\mu_n r) - \mu_n r K_1(\mu_n r) \right] \quad \text{(A32)}$$

$$g_{7n}^{(i)} = \frac{\mu_n^2}{r} K_1(\mu_n r) \quad \text{(A33)}$$

$$g_{8n}^{(i)} = \mu_n^3 \left(\frac{c_{11}^{(i)} - c_{12}^{(i)}}{c_{11}^{(i)} + c_{12}^{(i)}} \right) K_0(\mu_n r) \quad \text{(A34)}$$

$$g_{9n}^{(i)} = \mu_n^3 K_0(\mu_n r) \quad \text{(A35)}$$

$$g_{10n}^{(i)} = \mu_n^3 \left[\left(\frac{4c_{11}^{(i)} + 2c_{12}^{(i)}}{c_{11}^{(i)} + c_{12}^{(i)}} \right) K_0(\mu_n r) + \mu_n r K_1(\mu_n r) \right] \quad \text{(A36)}$$

$$g_{11n}^{(i)} = -\mu_n^3 K_1(\mu_n r) \quad \text{(A37)}$$

$$g_{12n}^{(i)} = \mu_n^3 \left[\left(\frac{4c_{11}^{(i)}}{c_{11}^{(i)} + c_{12}^{(i)}} \right) K_1(\mu_n r) - \mu_n r K_0(\mu_n r) \right] \quad \text{(A38)}$$

REFERENCES

Banno, H. 1983. "Recent Developments of Piezoelectric Ceramic Products and Composites of Synthetic and Piezoelectric Ceramic Particles", *Ferroelec.*, 50(1):3-12.

Cao, W., Q. M. Zhang and L. E. Cross. 1992. "Theoretical Study on the Static Performance of Piezoelectric Ceramic-Polymer Composites with 1-3 Connectivity", *J. Appl. Phys.*, 72(12):5814-5821.

Chan, H. L. W. and J. Unsworth. 1989. "Simple Model for Piezoelectric Ceramic/Polymer 1-3 Composites Used in Ultrasonic Transducer Applications", *IEEE Trans. Ultrason. Ferroelec. Freq. Contr.*, 36(4): 434-441.

Haun, M. J. and R. E. Newnham. 1986. "An Experimental and Theoretical Study of 1-3 and 1-3-0 Piezoelectric PZT-Polymer Composites Hydrophone Applications", *Ferroelec.*, 68(1):123-139.

Jensen, H. 1991. "Determination of Macroscopic Electro-Mechanical Characteristics of 1-3 Piezoceramic/Polymer Composites by a Concentric Tube Model", *IEEE Trans. Ultrason. Ferroelec. Freq. Contr.*, 38(6): 591-594.

Lees, S. and C. L. Davidson. 1977. "Ultrasonic Measurement on Some Mineral Filled Plastics", *IEEE Trans. Sonics Ultrason.*, SU-24:222-225.

Lekhnitskii, S. G. 1981. *Theory of Elasticity of an Anisotropic Body.* Mir Publishers.

Nairn, J. A. 1992. "A Variational Mechanics Analysis of the Stresses around Breaks in Embedded Fibers", *Mechanics of Materials*, 13(2):131-154.

Newnham, R. E. 1986. "Composite Electroceramics", *Ferroelec.*, 68(1): 1-32.

Whitney, J. M. and L. T. Drzal. 1987. "Axisymmetric Stress Distribution around an Isolated Fiber Fragment", *Toughened Composites, ASTM STP 937*, pp. 179-196.

Zhong, F. H. and E. S. Folias. 1992. "The 3D Stress Field of a Fiber Embedded into a Matrix and Subjected to an Axial Load", *Computational Mechanics*, 9:233-247.